Cell Reports
Physical Science

CellPress
OPEN ACCESS

Article

Membranous sheath of a fan worm functions as a high-performance energy absorber and stabilizer

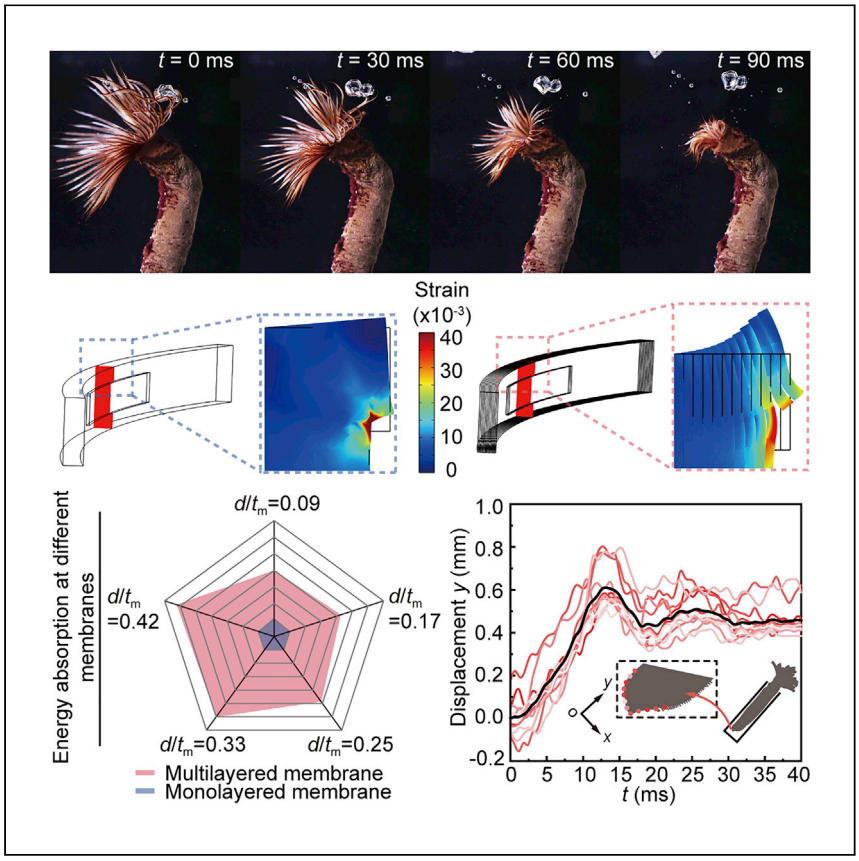

Inspired by a kind of marine worm, Bai et al. demonstrate a multilayer-structured material unique to worms that can simultaneously function as both a robust energy absorber and an efficient stabilizer. This soft material can further extend applications of multilayered materials in limited spaces or unstructured scenarios.

Siyu Bai, Shi-Yang Tang, Jianing Wu

s.tang@bham.ac.uk (S.-Y.T.)
wujn27@mail.sysu.edu.cn (J.W.)

Highlights

The membrane is solidified by biological mucus combined with substances in seawater

The membrane provides superior mechanical performance

The membrane can simultaneously function as an energy absorber and a stabilizer

An underwater biological anchorage system is proposed

Bai et al., Cell Reports Physical Science 4, 101253
February 15, 2023
https://doi.org/10.1016/j.xcrp.2023.101253

Cell Reports
Physical Science

CellPress
OPEN ACCESS

Article

Membranous sheath of a fan worm functions as a high-performance energy absorber and stabilizer

Siyu Bai,[1,2] Shi-Yang Tang,[3,*] and Jianing Wu[1,2,4,*]

SUMMARY

Multilayered structure at the macroscale is a prevailing pathway for developing high-performance energy absorbers. Nowadays, most multilayer-structure-based energy absorbers are constructed with rigid materials, but research on utilizing soft materials as energy-absorbing devices is still rare. By understanding the function of membranous sheathes in the stimuli responsiveness of fan worms (Polychaeta: *Sabellastarte australiensis*), in this work, we report a robust biological energy absorber made of multilayer-structured soft material. Our study reveals that structural features govern the mechanical performance and the energy-absorption capacity of this soft energy absorber. Ultimately, through kinematic analysis of fan worms, we elucidate the advantage of soft-material-based energy absorbers in stabilizing assistance compared with rigid counterparts. Our work takes a significant step toward understanding the design principle of soft-material-based energy absorbers and may shed light on flexible protective devices for soft robotics.

INTRODUCTION

Multilayered structures, generally featuring the merits of high strength, high stiffness, and high energy absorption rates,[1–6] have been widely used in diverse applications.[7–12] The high energy absorption rate is a predominant property of the multilayered structures that characterizes the performance of impact resistance.[13,14] However, most multilayered structures with high energy absorption rates are fabricated with rigid materials (Figure S1).[13] For example, Zou et al. developed a bioinspired multicelled tube energy absorber inspired by the structure of bamboo[15]; Signetti et al. proposed ceramic-composite panels inspired by fish scales for impact protection.[16] While these bioinspired rigid materials demonstrate excellent energy absorption capacities, their applications in limited spaces or unstructured environments are hindered.

In nature, multilayered structures are pervasive in plants and animals.[13,17–19] A fan worm (Polychaeta: *Sabellastarte australiensis*) is a marine polychaete worm living in unstructured interspaces of reefs and rocks. During filter feeding, it extends its crown-like tentacles but leaves the majority of its body in the multilayered soft membrane sheath (hereinafter referred to as membrane), which is mainly constructed by self-secreted mucus.[20] The fan worm can generate a biological stimuli responsiveness by swiftly retracting its body into the membrane for defense within 90 ms (Figure 1A).[21,22] To visualize the possible configurational variation of the worm body, we replace the membrane with a glass tube by a gentle approach (Note S1). Figure 1B uncovers profiles of the segmented worm body in the initial and final

[1]School of Advanced Manufacturing, Sun Yat-Sen University, Shenzhen, Guangdong 518107, P.R. China

[2]School of Aeronautics and Astronautics, Sun Yat-Sen University, Shenzhen, Guangdong 518107, P.R. China

[3]Department of Electronic, Electrical and Systems Engineering, University of Birmingham, Birmingham B15 2TT, UK

[4]Lead contact

*Correspondence: s.tang@bham.ac.uk (S.-Y.T.), wujn27@mail.sysu.edu.cn (J.W.)

https://doi.org/10.1016/j.xcrp.2023.101253

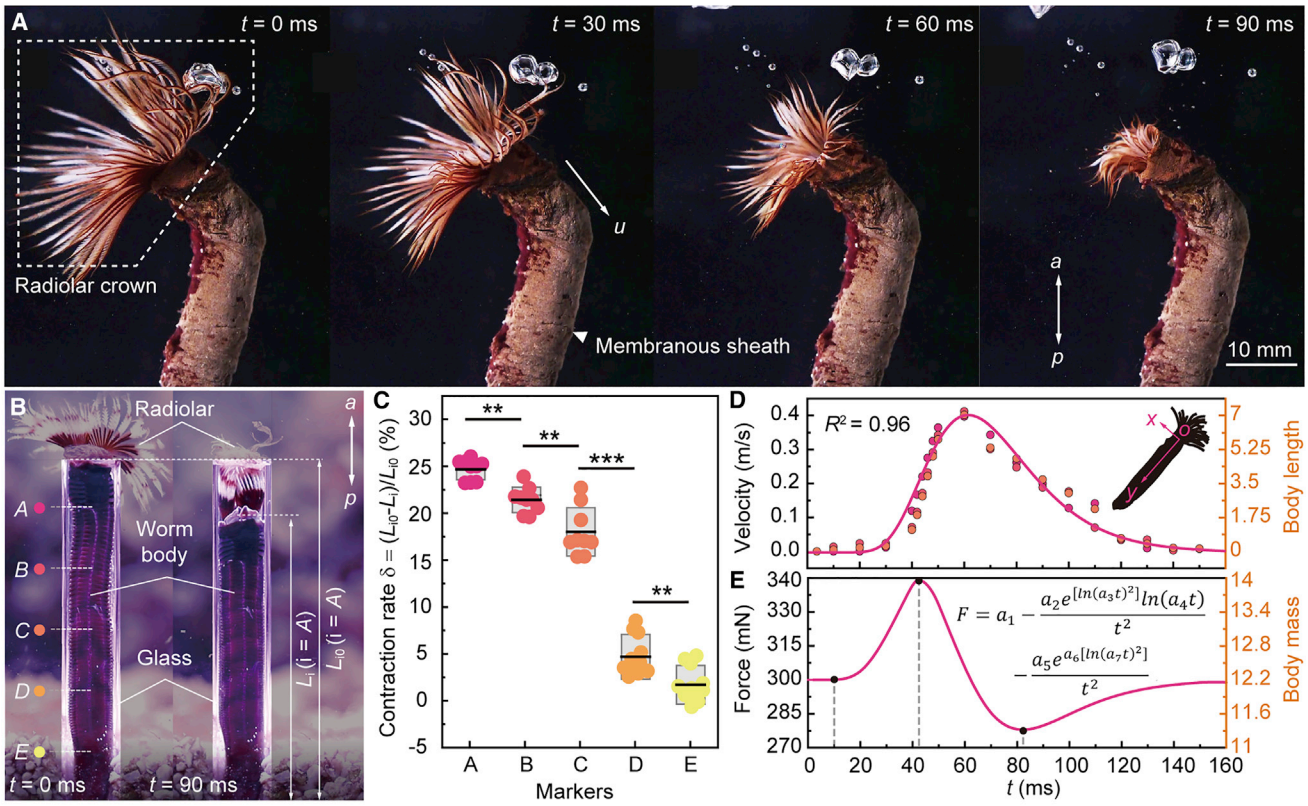

Figure 1. Ultrafast withdrawal of a fan worm through the membranous sheath

(A) Frame sequence of fast retraction of a fan worm indicated by an instantaneous retracting velocity *u*. *a*-*p*, antero-posterior axis.

(B) Morphology of the fan worm body observed through a glass tube, which shows the appearance of a fully extended body (left) and a fully contracted body (right).

(C) Contraction rates of five markers on the body. Significant differences are noted with star values, with the p values from left to right: **p = 0.022, **p = 0.020, ***p < 0.0001, and **p = 0.012. Black line: mean; gray box: SD. 9 worm samples.

(D) Retracting velocity of the fan worm with respect to time (top panel), where the experimental data can be fitted by logarithmic normal distribution with R^2 = 0.96.

(E) The force $F(t)$ exerting on the soft membrane during fast retraction (bottom panel).

stages of retraction. Compared with the starting time, the fully contracted worm body shortens by 20% in length. We measure the region-wise deformation of the worm body by carefully attaching five markers evenly distributed on the antero-posterior axis (*A*, *B*, *C*, *D*, *E*) to quantify the contraction rate of the body (Figure 1B), which is defined as

$$\delta_i = \frac{L_{i0} - L_i}{L_{i0}}, (i = A, B, C, D, E) \qquad \text{(Equation 1)}$$

where L_{i0} and L_i represent the distance from each point to the posterior body at t = 0 and 90 ms, respectively. As illustrated in Figure 1C, the contraction rate on the most anterior point is δ_A = 24.7%±1.1%, which is 14 times that of the most posterior point (δ_E = 1.7%±2.1%). The contraction rate monotonically decreases from the anterior part to the posterior part, which implies that the physics of rapid maneuver of a fan worm can be considered as a contractile soft body anchoring its posterior end to the soft membrane. To better quantify the rapid contraction of a fan worm and obtain the anchoring force on the membrane, we measure the retracting velocity of the fan worm in Figure 1D, which shows that the instantaneous retracting velocity of a fan worm can reach up to 7 body length/s (~400 mm/s). Furthermore,

based on a function $u(t)$ used to fit the retracting velocity (Figure 1D), the anchoring force (F) on the membrane can be calculated by

$$F(t) = m\frac{du(t)}{dt} + f - mg \quad \text{(Equation 2)}$$

where m is the weight of the worm body and f indicates the total resistance during retraction (Notes S3 and S4; Figure S11). Ultimately, Figure 1E shows that the force $F(t)$ exerting on the soft membrane arrives at a maximum value of F_{max} = 340 mN, which is ~14 times of body weight.

At such a high retracting velocity of fan worm and an enormous anchoring force on the membrane, the seemingly fragile soft membrane may have to overcome two challenges. The first is a huge anchorage force that may cause structural failure of both the worm body and the membrane. The second is the ultrafast speed-induced instability, which may lead to motion instability, thereby making its tender body collide with the posterior part of the tube. However, our careful check reveals that the worm body remains uninjured after repeated ultrafast locomotion and can also regain stability in a short period of ~35 ms.[23] Therefore, we speculate that the soft membrane has offered a potentially feasible solution to these challenges.

Previous literature only record the anatomy of the multilayered structure of the membrane.[20] In this study, we focus on the functions of the multilayered soft membrane in biological stimuli responsiveness and discuss how structural features contribute to the functional performance of the membrane by using a combined theoretical and experimental method. We demonstrate that the multilayered soft membrane is an integrated robust energy absorber and an efficient stabilizer, leading to a new function of multilayer-structured materials with potential applications in unstructured spaces. Thus, this work may not only provide guidelines for the design principle of multilayered soft materials but also inspire structural materials for broader engineering applications.

RESULTS AND DISCUSSION

Material properties of the membrane

To illustrate the anchoring mode between the membrane and the fan worm, we examine the morphology of the fan worm and the internal surface of the membrane interacting with the worm body. Through the glass tube, we can find a newly secreted membrane that parcels up the worm body (Figures 2A and S2). As illustrated in the scanning electron microscopy (SEM) images given in Figure 2B, the hooks form a tightly packed transverse row in each torus and make the hooks point opposite to the direction of the fan worm's retraction. The enlarged view of an individual hook shown in Figure 2B indicates that the fan worm hooks possess specific directivity and can only achieve unidirectional anchorage. The hooks are known to have the primary function of resisting the removal of worms from their membranes[23]; however, previous studies poorly understood the physical interaction between hooks and membranes. Our high-speed frames show that the elongated anterior part of the body detaches the hooks from the membrane, while the posterior part of the body attaches the hooks to the membrane (Figure S3; Video S1).

Figure 2C shows the SEM image revealing a cross-section of the multilayered membrane, where the total thickness the of 12-layered membrane is t_m = 60 ± 5 μm with each lamella (one layer of membrane) having a thickness of t_l = 5.03 ± 0.50 μm on average (Figure S4). The fan worm continuously secretes mucus at a production rate of 1–2 min per layer, which eventually forms the multilayered membrane.[24,25]

An older membranous sheath is thicker and stronger than a newly formed one and has a higher number of layers. In addition, the fan worm is not sedentary because it will readily evacuate its membranous sheath and can quickly form another. Through our observations, we can continually find that the fan worm jettisons the old sheath and replaces it with a newly secreted one. To identify the anchorage between the posterior part of the hooks and the membrane, we examine the inner surface of the membrane using SEM. We discover that transversely distributed cracks, which have an average length of $a = 32.33 \pm 6.87$ μm and an average width of $b = 3.40 \pm 0.43$ μm, are morphologically consistent with the distribution principle of the hooks (Figure 2D).

According to morphology of the hooks and cracks, we draw the hooks-membrane apparatus in the coordinates xyz shown in Figure 2E. The first schematic from the left illustrates the basic morphology of a fan worm viewed on its longitudinal cross-section. The second schematic illustrates two rows of hooks on a cross-section, with a row of hooks and a corresponding crack highlighted by a blue box, which is magnified in the third schematic. In this article, only one crack is involved in designing the model since the hooks of the fan worm are distributed in two longitudinal columns on both sides of the body and circumferential distance between the two columns is ~1.3 cm, which is about 5 times the length of one crack.[26,27] At this scale, the interaction between the two longitudinal columns of hooks can be negligible. Furthermore, our simulations validate that the mechanical properties of two adjacent cracks in one column hardly interfere with each other (Figure S5). This leads to independence in the mechanical property of each crack, which allows us to simplify the model merely considering one crack interacting with one row of hooks.

Using energy-dispersive spectroscopy (EDS), we examine the material composition of the membrane and confirm that seven primary elements—carbon, oxygen, magnesium, silicon, sulfur, calcium, and cobalt—compose the membrane surface (Figures 2F and S6). These elements have distinct mass percentages in the membrane, showing a biomaterial abundance in organic matter and carbonates. The organic matter primarily might be acid mucopolysaccharide-protein complexes from viscous mucus secreted by the worm,[28] while the carbonates that allow the construction of the mineralization tube might be collected from debris (i.e., mineral grains) cemented with mucus.[24,26] In addition, metals in seawater might accumulate in the membrane upon the process of tube formation and growth, which is bound to mucus and sediment particles.[27] The combination of the substances mentioned above with the surface membrane significantly improves the mechanical properties of the fan worm membrane and contributes to damage resistance caused by external forces.[29] For the specimens of fan worms, the tensile limit of the membrane (i.e., the weight needed to tear the sheath) can reach up to 800 g, which is 400 times the body weight.[30]

To examine the mechanical properties of such a composite biomaterial, we perform tensile tests on the membrane. The experimental schematic diagram is shown in the inset of Figure 2G, and basic parameters can be found in Table S1. The curve demonstrates a peak, corresponding to the fracture of the membrane, indicating that the tensile strength of the membrane is $\sigma_t = 1$ MPa. The stress-strain curve has a linear region when $\varepsilon < 0.20$ or $\sigma < 0.9$ MPa; it is thus reasonable to suggest that the membrane is linearly elastic. Figure 2G shows that the membrane has an average Young's modulus of $E = 6 \pm 0.7$ MPa, which indicates that the membrane has a stiffness close to spring-like biomaterials such as poly (ε-caprolactone) fibers.[31,32] To further verify

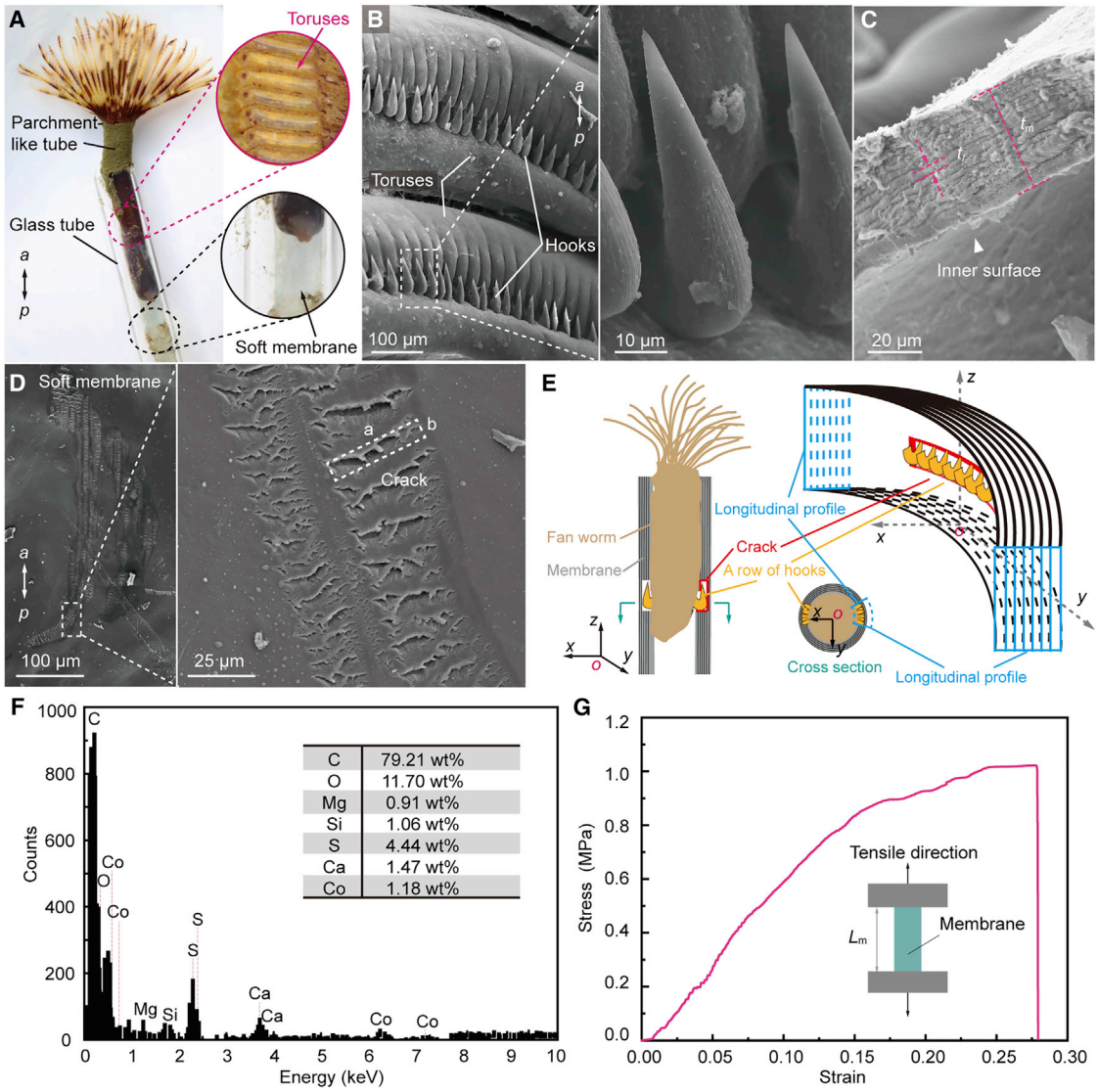

Figure 2. Morphology of the hooks and soft membrane of a fan worm

(A) The fan worm fully extended and anchored posteriorly. *a-p*, antero-posterior axis.

(B) SEM images of hooks bearing on surface of toruses. The enlarged portion shows the appearance of a single hook.

(C) A fractured cross-section of a membrane. t_m, thickness of the membrane; t_l, thickness of the lamella.

(D) SEM images of the membrane surrounding the posterior body show the inner surface with highly dense traces aligning along the long axis of the body. The zoomed-in image shows the appearance of the cracks.

(E) Schematics showing the hooks-membrane apparatus composed of the hooks and the multilayered membrane. In the xyz coordinates, z is in alignment with the long axis of the fan worm, and *xoy* represents the cross-section of the fan worm.

(F) EDS spectrum of the membrane and elemental concentrations (inset).

(G) Stress-strain curve of the fresh membrane examined by tensile testing. Schematic diagram of tensile testing (inset).

the tensile test, Young's modulus of the membrane surface is measured by atomic force microscopy (AFM) (Figure S7). The difference between the tensile and AFM tests is about 8.3%, which validates the accuracy of the tensile tests.

A numerical model composed of multilayered membranes with a crack (length of *a*, height of *b*, and depth of *d*; see Figure S8 and Table S2 for details) is built to characterize a row of hooks anchoring the membrane (Figure 2E). To understand how the lamella thickness reveals the robustness of the membrane, we first set up a series

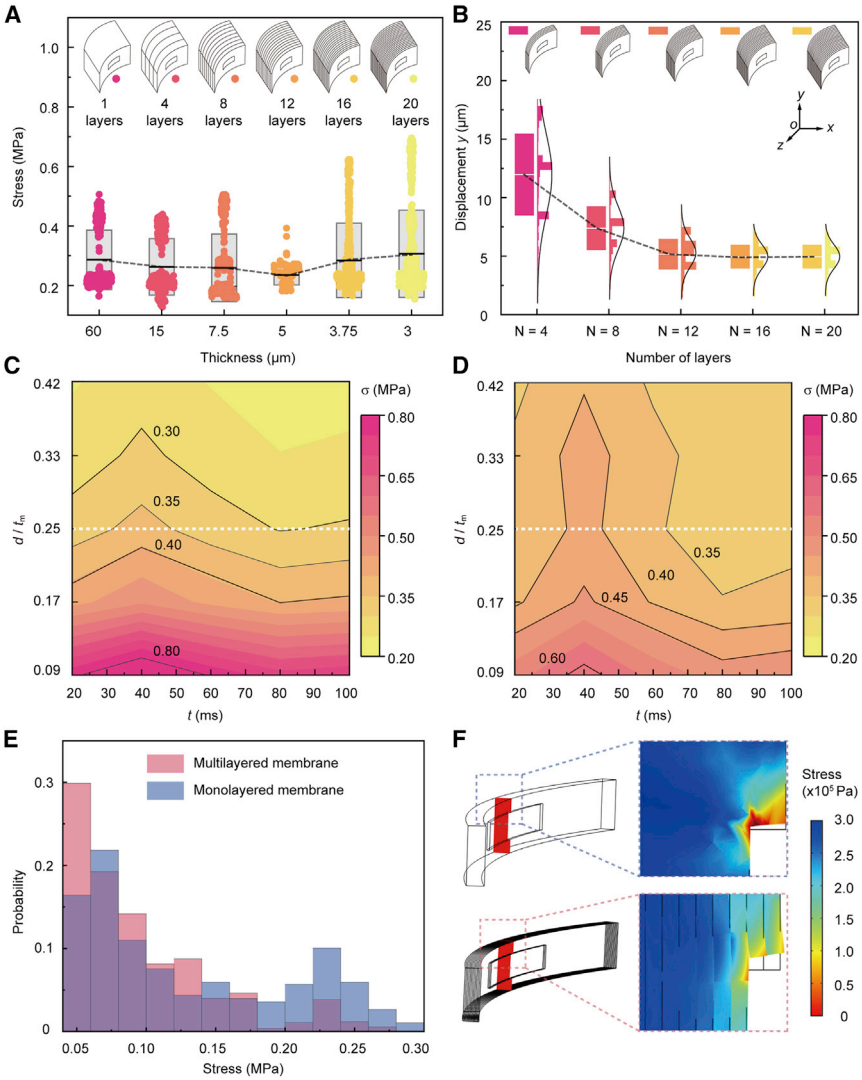

Figure 3. Material properties and mechanical performance of the soft membrane

(A) Stress distribution of the membrane cracks under both fixed total thickness of 60 μm and anchorage depth of 10 μm for a range of lamella thicknesses.

(B) Longitudinal deformation of the upper surface of the crack for membranes with different layers, where *j* indicates the number of layers.

(C and D) Contour plots of the stress in MOM and MUM models, the ratio of the anchorage depth to membrane thickness, and force *F* against time, respectively.

(E) Probability distributions of stress of upper edges of the cracks on MOM and MUM models, respectively.

(F) Local stress distributions of monolayered and multilayered membranes in the case of d/t_m = 0.17 at t = 42 ms.

of membrane models with varying lamella thickness (MVLTs) and a crack (100 × 10 × 10 μm), respectively dividing membrane models of t_m = 60 μm into N lamellae (N = 1, 4, …, 20). By applying a normal force of F_{max} to the upper edge of the crack with a fixed bottom and outer surfaces of the membrane model (Figure S8), we make a statistical analysis of the stress magnitudes of the upper edge and uncover the relationship between stress and lamella thickness $t_l = t_m/\mathrm{N}$ in Figure 3A. Numerical results indicate that the average stress exhibits an optimal lamella thickness of t_l = 5 μm (12 layers of lamella) that leads to the minimum stress. Notably, such an optimum is close to the natural lamella thickness, which is 5.03 ± 0.50 μm extracted from

the SEM images, and implies the concordance between the theoretical optimum and natural design. In addition to the lamella thickness, the number of lamellae layers may also impact the structural strength of the membrane. We then create membrane models with a varying number of lamellae (MVNLs), noted as N ranging from 4 to 20 with an increment of 4 and a constant lamella thickness of t_l = 5 μm. To determine the effect of total thickness on model deformation, we remove the fixed constraint on the outermost surface of the membrane while keeping the other settings unchanged compared with MVLTs. Numerical results show that the average displacement y of the upper edge of the crack monotonically decreases and plateaus as N approaches 12, which suggests a critical lamella number of N = 12 for marginal benefit in terms of displacement y (Figure 3B). The decreasing displacement y can effectively reduce the deformation of the soft membrane and the possibility of structural failure at the anchoring position. Therefore, combining the finite-element analysis on MVLTs and MVNLs, the characteristic case with N = 12 and t_l = 5 μm can be featured.

Generally, the mechanical performance and structural robustness of the membrane are mediated by the trade-off between anchorage depth and the thickness of the substrate. Therefore, anchorage depth may be applied to identify critical risks for stability,[33,34] which may directly impact the success of anchoring and the stress distribution of the membrane. For fan worm anchorage, the anchorage depth can be characterized by the ratio of crack depth d to membrane thickness t_m, yielding the characteristic depth d/t_m. We can thus increase the characteristic depth from 0.09 to 0.42 with an increment of 0.08 to investigate the impact of characteristic depth on the stability of hook anchorage. We build the monolayered membrane (MOM) models (N = 1 and t_l = 60 μm) and the multilayered membrane (MUM) models (N = 12 and t_l = 5 μm) with varying d/t_m (Table S2). Our numerical simulation results show that both the maximum stress of MOM and MUM models decreases with an increasing d/t_m. For instance, if d/t_m = 0.42, MOM models predict a maximum stress of σ_{mon} = 0.25 MPa at t = 42 ms, which is 71% of the maximum stress σ_{mul} of MUM models. For comparison, as the characteristic depth declines to 0.09, we get an increased stress σ_{mon} = 0.8 MPa, which is 1.5 times σ_{mul} (Figures 3C and 3D). Figure 3E shows the probability distributions of the stress on the MOM and MUM models under the condition of d/t_m = 0.17 and t = 42 ms. The numerical results predict the probability when σ_{mon} > 0.18 MPa is 2.34 times the case of σ_{mul} > 0.18 MPa. A stress over 0.18 MPa usually occurs at the crack tip, implying that MUM models are more beneficial to avoid damage accumulation and failure caused by fatigue during repeated anchoring compared with MOM models (Figure 3F). Therefore, for fan worms, the specialized structure of the MUM increases the mechanical performances of the anchorage structure.

A combined energy absorber and stabilizer

A MUM can be considered a spring-like structure that may support buffering rapid withdrawal of fan worms.[35] To better understand the buffering performance of the membrane in the fan worm, the MOM and MUM models in response to anchorage can be respectively simulated by applying $F(t)$ to the cracks of different characteristic depths. As time t increases from 0 to 160 ms, we can obtain the force exerted on the upper edge of the crack as a function of displacement y during the anchorage process. The force-displacement response F_y of the upper edge of the crack can be found in Figure 4A, which compares the results of MOM and MUM models. We linear fit all the points of MOM and MUM models with different d/t_m and calculate the equivalent spring stiffness of the elastic membrane. The average equivalent spring stiffness of MUM models is k_{mul} = 345±63 kN/m, which is merely 23% of that of

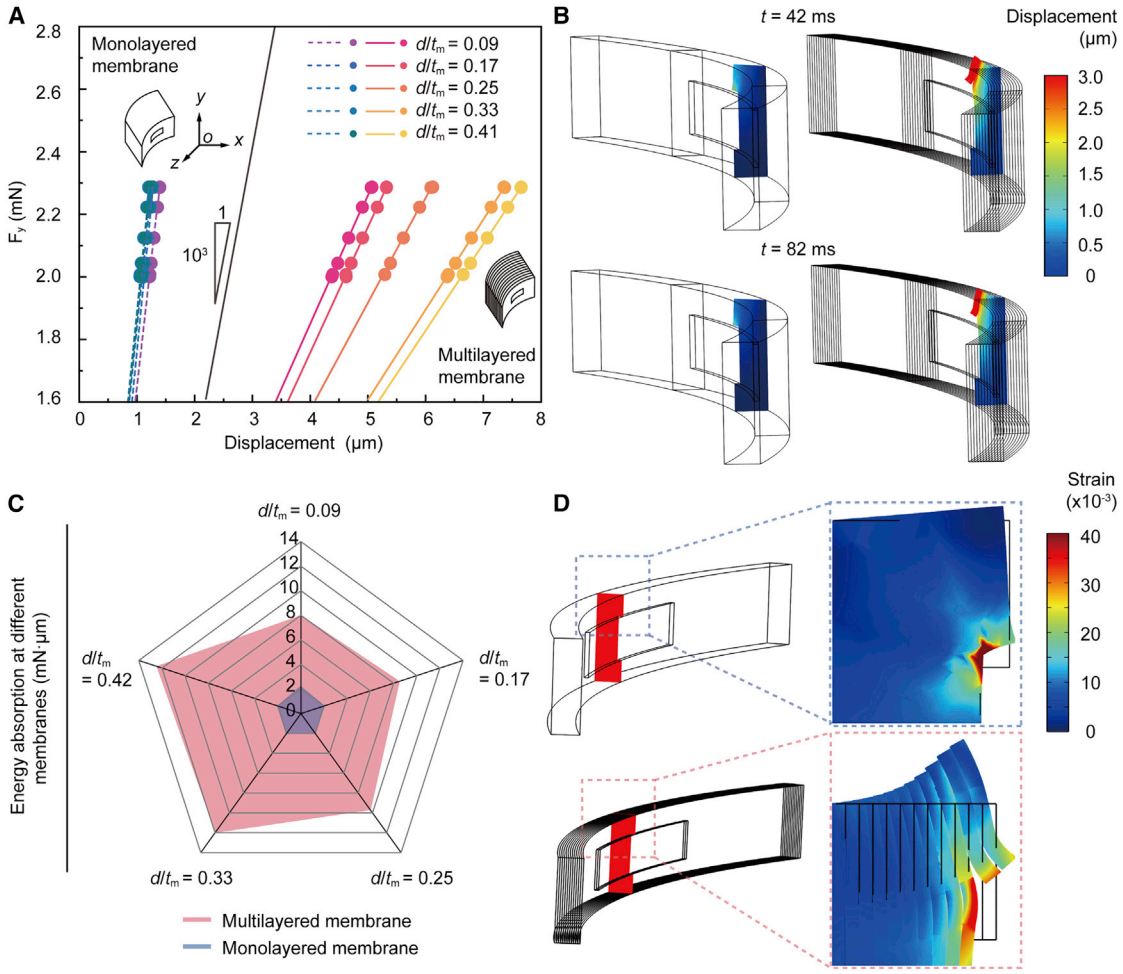

Figure 4. Energy-absorption simulation

(A) The force F_y subjected to the upper edge of the crack is a function of the maximum displacement along the axial direction (y axis).

(B) Displacements of the two comparative models.

(C) Energy absorption of MON and MUM models under variable characteristic depths d/t_m.

(D) Local strain distributions of monolayered and multilayered membranes for the case of d/t_m = 0.17 at t = 42 ms.

MOM models (k_{mon} = 1,794±94 kN/m), suggesting that MUM has a lower stiffness to facilitate energy absorption by generating larger deformation.[36]

Figure 4B shows the displacements of MOM (left) and MUM (right) models caused by $F(t)$ at t = 42 and 82 ms. The numerical results suggest that the maximum deformation of the cracks α of the MUM models is 3.6 times that of the MOM models. The energy absorption of MOM and MUM models at different d/t_m can be calculated as $W = \int_0^{\alpha} F(y)dy$, which is illustrated as a radar map in Figure 4C. The blue octagon entirely lays inside the red one, suggesting that MUM models are more conducive to energy absorption than MOM models. When d/t_m = 0.42, the energy absorption by MUM is 6 times that of MOM, implying that the energy dissipation can be greatly increased if MUM is employed, which might be caused by the interlayer slippage of lamellae (Figure 4D).[37,38]

To unveil the potential advantages of the energy absorber made of the soft membrane, we turn to investigate the posterior-body dynamics during a fast retraction

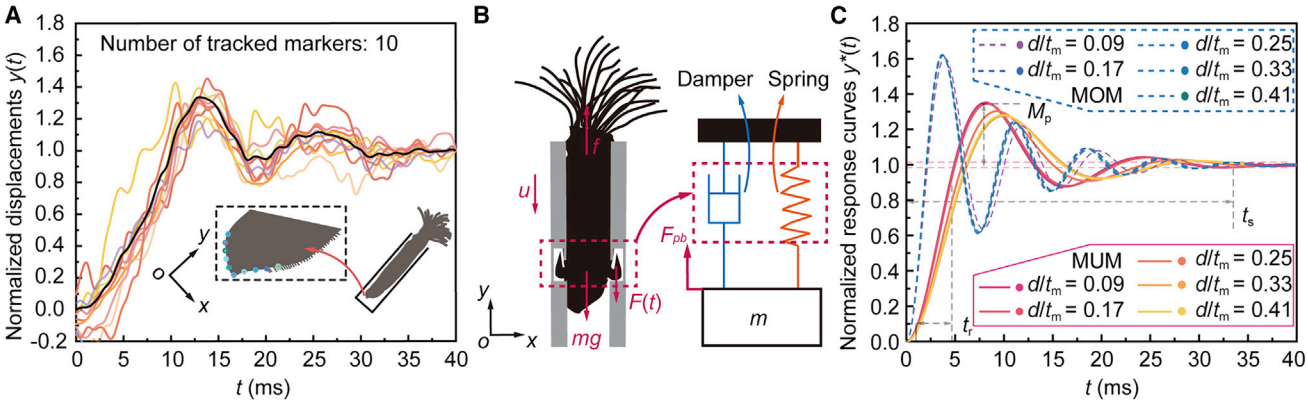

Figure 5. Damping effects of the fan worm for motion stabilization

(A) Position of 10 markers (red points) distributed on periphery of the posterior body as the posterior body oscillates. Chromatic curves show normalized displacements of markers in the y direction, and the black line exhibits the averaged normalized displacement of them. O is the origin of the Cartesian (x and y) coordinate fixed at the posterior body.

(B) One-degree-of-freedom system relying on the hooks-membrane apparatus.

(C) Normalized response curves of MOM and MUM models. Parameters: t_r, rise time; t_s, the setting time; M_p, maximum overshoot.

of the fan worm body into the membranous sheath, which may not only cause a high impact on the membrane but could also challenge kinematic stability of the worm body. High-speed images indicate that the posterior body anchors the membrane by hooks and displays an oscillatory fashion until reaching the equilibrium state (Figure 5A; Video S1). The continuous retardation of the soft MUM allows the kinetic energy of the fan worm to be released gradually rather than dissipated by instantaneous impact as in rigid materials. This unique advantage of the soft membrane may explain why fan worms can perform ultrafast retraction repeatedly without causing structural damage to the membrane. However, such an oscillation is common in governing maneuvers, requiring the damping force to brake.[39] This suggests that using multilayered soft materials as an energy absorber may offer other potential advantages over rigid materials, namely that the membrane simultaneously functions as a stabilizer.

The high-speed recordings show that, throughout the oscillation, the posterior body and the inner surface of the membrane remain in contact. To characterize the functionality of the multilayered soft membrane, we model the worm body and membrane as a one-degree-of-freedom system (a second-order system). Figure 5B shows the schematic diagram of our theoretical model in which the membrane simultaneously functions as a damper and a spring. Ulteriorly, a transfer function is established to describe the system's response to the perturbation of external force $F_{pb} = f - mg$, which demonstrates the response characteristics and the system stability (Figure S9; Note S5; Table S4). Figure 5C shows the normalized unit-step response curves $y^*(t)$ of MUM and MOM.

The dynamic behaviors of an oscillation system can be then described in terms of two parameters: the damping ratio ξ and the undamped natural frequency (corner frequency) ω_n.[38] To highlight the superiority of multilayered soft membrane as a stabilizer compared with MOM, we analyze the posterior-body oscillation characteristics of the fan worm in MOM and MUM. Both ξ_{mon} and ξ_{mul} are less than 1, which shows an underdamped oscillation (Table S3). However, $\xi_{mon}/\xi_{mul} \sim (k_{mul}/k_{mon})^{1/2} = 0.44$ suggests that the MOM oscillator contributes a lower ξ. In addition, comparing the normalized unit-step response curves $y^*(t)$ of the two oscillators shown in

Figure 5C, the MOM has a ~2 times higher corner frequency ω_n than the MUM. Generally, an oscillation system with a lower ξ and higher ω_n produces a shorter rise time t_r and improves the overshoot M_p in response, which may lead to a reduction in stability.[38] Figure 5C shows that the M_p and t_r of the MOM oscillator are about 1.5 and 2.3 times those of the MUM oscillator, respectively. Under the same setting time t_s, the MOM oscillator produces a higher frequency and a larger amplitude than the MUM oscillator in the process of restoring stability, which increases the possibility of fatigue fracture of the membrane. Thus, we demonstrate that the multilayered soft membrane of fan worm not only functions as an energy absorber like other lamellar structures readily appearing in biological shells or exoskeletons but also takes full advantage of soft materials to construct a damping system to assist the fan worm in maintaining body stability.[40–43] Finally, this modeling approach may be widely applicable to other fan worm species whose functional morphologies are similar to the modeling species (*S. australiensis*), capable of making fast retraction through membranous sheaths.

In this study, based on the rapid retraction of a fan worm, we present the structural and functional challenges of materials caused by high-speed movement in a narrow space. However, the fan worm membrane with a unique multilayered structure provides a robust yet stable substrate through which the membrane can not only resist thousands of strokes but can also assist the fan worm in regaining stability after ultrafast retraction. In this study, we reveal how the soft membrane functions as a robust energy absorber and how the MUM functions as an efficient stabilizer during fast retraction of the fan worm.

Our study elucidates that such a membrane needs to have great mechanical properties for its proper function. Combining kinematics of the fan worm, mechanical testing of the membrane, and finite element analysis, we can summarize that a membrane with specific lamella thickness, lamella number, and structural stiffness can yield optimized mechanical properties in response to anchored load. Such knowledge helps understand the principle of a multilayer-structured design and may provide a paradigm for anchorage devices used in unstructured environments.

Moreover, benefiting from the nonrigid multilayered construction, the fan worm and the membrane can be considered a one-degree-of-freedom system, exhibiting multiple oscillations over a very short timescale. Notably, the membrane makes the fan worm restore stability by dissipating the excess kinetic energy. Moreover, the multilayered configuration has a significant advantage in reducing both amplitude and frequency of the oscillatory motion compared with the monolayered configuration. Nevertheless, the potential of a multilayered structure to function as a stabilizer has not been fully explored in previous research. Further insights into this soft yet resilient membrane can be favorable for developing a stability-auxiliary device potentially applied in deep-sea sensors and pipeline robots.[44,45]

EXPERIMENTAL PROCEDURES

Resource availability

Lead contact

Further information and requests for resources should be directed to and will be fulfilled by the lead contact, Jianing Wu (wujn27@mail.sysu.edu.cn).

Materials availability

This study did not generate new unique materials.

Data and code availability

All experiment data are available upon reasonable request to the lead contact.

Animal cares

Six fan worms were housed in an aquarium (600 × 500 × 350 mm) with an entire reef rock ecosystem that was kept at Sun Yat-Sen University, Shenzhen, China (23° N, 113° E). We prepared seawater by adding sea salt (sodium chloride) into purified water at a mass ratio of 25‰ and kept the temperature at 25°C by an automatic heater, then raised some marine plants in the aquarium to simulate the living environment of fan worms. An illuminator (120 W, 12,000 K) was employed to simulate sunlight exposure. We confirmed that no specific permissions were required for these locations/activities, and the studies did not involve endangered or protected species.

High-speed imaging

We kept fan worms treated as in Note S1 inside a smaller tank (15 × 15 × 20 cm) filled with seawater and triggered their evacuation response by jetting water on their radioles. A high-speed camera (Phantom, VEO 340L, NJ, USA) equipped with a micro-lens (Canon, CX33, Tokyo, Japan) recorded the retraction of the fan worm at a frame rate of 1,000 fps. After that, we used the high-speed camera coaxially connected to a microscope (Olympus, CX33, Tokyo, Japan) to film movements of the posterior end of the fan worm body at a frame rate of 1,000 fps (Note S2). All videos were then processed via the software of Phantom Camera Control 3.3 (Vision Research, Wayne, NJ, USA) and Tracker 4.9.1 (copyright Douglas Brown, USA).

SEM and EDS

Six pieces of fresh membranes attached to the inner surface of the natural membrane and four pieces of muscular tissues with the fan worm hooks bearing on them were dehydrated respectively in a graded series of ethanol (70%, 80%, 90%, 96%, and 100%, 15 min each) and dried for 12 h in a desiccator using 1-propanol. The specimens were analyzed using SEM (EVO MA10 SEM, ZEISS, Oberkochen, Germany) and EDS (Merlin Compact, Carl Zeiss, Jena, Germany).

Tensile test

We cut fresh membrane samples for tensile testing into rectangular pieces with a scalpel (Table S1). Next, we clamped each end of the sample with two pieces of cardboard using tweezers, which limited the possibly of sliding between the specimen and the clamp during tensile testing. As shown in Figure 2G, the sample was fixed by tensile tester clamps before testing. For each fresh specimen, there was a 15-min limit on each specimen preparation to make sure the inherent mechanical properties of the natural membrane of the fan worm could be recorded. In this test, the speed of the tensile tester was set to 0.523 mm/s, and the stress-tension data could be captured in real time.

AFM

We used scissors to gently cut a 2×2 cm sample from the natural membrane and mounted it on a glass slide coated with a uniform epoxy resin adhesive (Deli, Ningbo, China). Notably, all preparation procedures were conducted at the temperature of 25°C and a humidity of 60% to ensure that the water content in the sample was kept stable. An AFM (Bruker, Karlsruhe, Germany) and a PFQNM-SMPKIT-12M probe (Bruker, Karlsruhe, Germany) were used to measure Young's modulus of the membrane in the marine environment. We employed the tap mode with a scanning

rate of 0.2–0.5 Hz and 256×256 pixel image. Since the indentation depth of the probe is only 0.17% of the sample thickness, it is reasonable to ignore the influence of epoxy resin glue as the substrate.

Finite element analysis

Four simulation cases of three-dimensional models mimicking fan worm membranes were established using computer-aided design software SolidWorks (v.2020, Dassault, France). These models were all composed of one or multiple layers of lamellae used to reveal the advantages of a natural membrane multilayered structure. In addition, to substitute the crack staying on the natural membrane interlocked with hooks, all models were built with cracks matching the natural conditions, namely the size and position of the traces (Figures S8 and S10). Four simulation cases were termed MVLTs, MVNLs, MUMs, and MOMs. Specific parameters for the four simulation cases can be found in Table S2. Then, the above models were imported into the solid mechanics module of the finite element software COMSOL Multiphysics (v.5.6, COMSOL, Stockholm, Sweden), and the material had a Young's modulus of 5 MPa, a Poisson's ratio of 0.3, and a density of 1,070 kg/m^3. Ultimately, this study only focused on the rapid retraction process of the fan worm, which is accomplished within ~160 ms. Considering the transient nature of this process, the possible influence of long-term stress on the crack propagation can be negligible. Therefore, none of the simulations emulating the crack propagation are involved in this article. More details about finite element analysis can be found in Notes S6–S9 and Figure S12.

SUPPLEMENTAL INFORMATION

Supplemental information can be found online at https://doi.org/10.1016/j.xcrp.2023.101253.

ACKNOWLEDGMENTS

This work was supported by the National Natural Science Foundation of China (grant nos. 51905556 and 52275298), the Grant for Popularization of Scientific and Technological Innovation of Guangdong Province (grant no. 2020A1414040007), and the Shenzhen Science and Technology Program (grant nos. GXWD20201231165807008 and GXWD20200830220051001). S.-Y.T. is grateful for the support from the Royal Society (IEC/NSFC/201223).

AUTHOR CONTRIBUTIONS

S.B., S.-Y.T., and J.W. conceived the idea and designed the study. S.B. designed and performed the experiments. S.B. completed finite element simulation and theoretical modeling. S.B. analyzed the data and wrote the manuscript. S.-Y.T. and J.W. provided valuable advice and supervised the research. All authors discussed the results.

DECLARATION OF INTERESTS

The authors declare no competing interests.

Received: October 11, 2022
Revised: November 28, 2022
Accepted: January 4, 2023
Published: January 25, 2023

REFERENCES

1. Tang, Z., Kotov, N.A., Magonov, S., and Ozturk, B. (2003). Nanostructured artificial nacre. Nat. Mater. *2*, 413–418.
2. Rubner, M. (2003). Synthetic sea shell. Nature *423*, 925–926.
3. Lu, G., and Yu, T.X. (2003). Energy Absorption of Structures and Materials (Elsevier).
4. Alghamdi, A.A.A. (2001). Collapsible impact energy absorbers: an overview. Thin-Walled Struct. *39*, 189–213.
5. Jones, N. (2011). Structural Impact (Cambridge university press).
6. Zhang, W., Deng, Z., Yuan, H., Luo, S., Wen, H., and Liu, T. (2021). Preparation and properties of silicone rubber materials with foam/solid alternating multilayered structures. Polym. J. *53*, 619–631.
7. Behera, R.P., and Le Ferrand, H. (2021). Impact-resistant materials inspired by the mantis shrimp's dactyl club. Matter *4*, 2831–2849.
8. Decher, G. (1997). Fuzzy nanoassemblies: toward layered polymeric multicomposites. Science *277*, 1232–1237.
9. Tang, L., Shang, J., and Jiang, X. (2021). Multilayered electronic transfer tattoo that can enable the crease amplification effect. Sci. Adv. *7*, eabe3778. https://doi.org/10.1126/sciadv.abe3778.
10. Luryi, S. (1988). Electronic devices using multilayer structures. In Physics, Fabrication, and Applications of Multilayered Structures (Springer), pp. 241–270.
11. Feraboli, P., Wade, B., Deleo, F., and Rassaian, M. (2009). Crush energy absorption of composite channel section specimens. Compos. Appl. Sci. Manuf. *40*, 1248–1256.
12. Ahmad, Z., Zhang, H.B., Farook, U., Edirisinghe, M., Stride, E., and Colombo, P. (2008). Generation of multilayered structures for biomedical applications using a novel tri-needle coaxial device and electrohydrodynamic flow. J. R. Soc. Interface *5*, 1255–1261.
13. Ha, N.S., and Lu, G. (2020). A review of recent research on bio-inspired structures and materials for energy absorption applications. Compos. B Eng. *181*, 107496.
14. Yang, T., Jia, Z., Chen, H., Deng, Z., Liu, W., Chen, L., and Li, L. (2020). Mechanical design of the highly porous cuttlebone: a bioceramic hard buoyancy tank for cuttlefish. Proc. Natl. Acad. Sci. USA *117*, 23450–23459.
15. Zou, M., Xu, S., Wei, C., Wang, H., and Liu, Z. (2016). A bionic method for the crashworthiness design of thin-walled structures inspired by bamboo. Thin-Walled Struct. *101*, 222–230.
16. Signetti, S., and Pugno, N.M. (2014). Evidence of optimal interfaces in bio-inspired ceramic-composite panels for superior ballistic protection. J. Eur. Ceram. Soc. *34*, 2823–2831.
17. Quan, H., Yang, W., Lapeyriere, M., Schaible, E., Ritchie, R.O., and Meyers, M.A. (2020). Structure and mechanical adaptability of a modern elasmoid fish scale from the common carp. Matter *3*, 842–863.
18. Yao, H., Dao, M., Imholt, T., Huang, J., Wheeler, K., Bonilla, A., Suresh, S., and Ortiz, C. (2010). Protection mechanisms of the iron-plated armor of a deep-sea hydrothermal vent gastropod. Proc. Natl. Acad. Sci. USA *107*, 987–992. https://doi.org/10.1073/pnas.0912988107.
19. Lin, A.Y.-M., and Meyers, M.A. (2009). Interfacial shear strength in abalone nacre. J. Mech. Behav. Biomed. Mater. *2*, 607–612.
20. Vinn, O., Zatoń, M., and Tovar-Hernández, M.A. (2018). Tube microstructure and formation in some feather duster worms (Polychaeta, Sabellidae). Mar. Biol. *165*, 98. https://doi.org/10.1007/s00227-018-3357-4.
21. Bok, M.J., Porter, M.L., and Nilsson, D.-E. (2017). Phototransduction in fan worm radiolar eyes. Curr. Biol. *27*, R698–R699.
22. Bok, M.J., Capa, M., and Nilsson, D.-E. (2016). Here, there and everywhere: the radiolar eyes of fan worms (Annelida, Sabellidae). Integr. Comp. Biol. *56*, 784–795.
23. Woodin, S.A., and Merz, R.A. (1987). Holding on by their hooks: anchors for worms. Evolution *41*, 427–432. https://doi.org/10.2307/2409149.
24. Bonar, D.B. (1972). Feeding and tube construction in chone mollis bush (polychaeta, sabellidae). J. Exp. Mar. Biol. Ecol. *9*, 1–18.
25. Vinn, O., Zatoń, M., and Tovar-Hernández, M.A. (2018). Tube microstructure and formation in some feather duster worms (Polychaeta, Sabellidae). Mar. Biol. *165*, 98.
26. Arias, A., Giangrande, A., Gambi, M.C., and Anadon, N. (2013). Biology and new records of the invasive species Branchiomma bairdi (Annelida: sabellidae) in the Mediterranean Sea. Mediterr. Mar. Sci. *14*, 162–171.
27. Lušić, J., Cvitković, I., Despalatović, M., Žunec, A., and Žuljević, A. (2022). Mediterranean fanworm, Sabella spallanzanii (Gmelin, 1791), as a potential biomonitor of trace metal pollution in the marine Environment. Chemosphere *287*, 132123.
28. Nicol, E.A.T. (1931). XXIII.—the feeding mechanism, formation of the tube, and physiology of digestion in sabella pavonina. Trans. R. Soc. Edinb. *56*, 537–598.
29. Bouligand, Y. (2004). The renewal of ideas about biomineralisations. Comptes Rendus Palevol *3*, 617–628.
30. Giangrande, A., Licciano, M., Schirosi, R., Musco, L., and Stabili, L. (2014). Chemical and structural defensive external strategies in six sabellid worms (Annelida). Mar. Ecol. *35*, 36–45.
31. Sun, Y., Zhang, J., Tang, X., Wu, Z., Gorb, S.N., and Wu, J. (2021). Specialized morphology and material properties make a honey bee tongue both extendible and structurally stable. Acta Biomater. *136*, 412–419.
32. Fleischer, S., Feiner, R., Shapira, A., Ji, J., Sui, X., Daniel Wagner, H., and Dvir, T. (2013). Spring-like fibers for cardiac tissue engineering. Biomaterials *34*, 8599–8606.
33. Bal, K.D., Bouma, T.J., Buis, K., Struyf, E., Jonas, S., Backx, H., and Meire, P. (2011). Trade-off between drag reduction and light interception of macrophytes: comparing five aquatic plants with contrasting morphology. Funct. Ecol. *25*, 1197–1205.
34. Lemieux, G., Hart, A., Cheretakis, C., Goodmurphy, C., Trexler, S., McGary, C., and Retrouvey, J.-M. (2011). Computed tomographic characterization of mini-implant placement pattern and maximum anchorage force in human cadavers. Am. J. Orthod. Dentofacial Orthop. *140*, 356–365.
35. Chen, D., Zhang, Z., and Chen, K. (2016). Legs attitudes determination for bionic locust robot based on landing buffering performance. Mech. Mach. Theor. *99*, 117–139.
36. Lakes, R., and Elms, K. (1993). Indentability of conventional and negative Poisson's ratio foams. J. Compos. Mater. *27*, 1193–1202.
37. Lei, Y., and Leng, Y. (2011). Stick-slip friction and energy dissipation in boundary lubrication. Phys. Rev. Lett. *107*, 147801.
38. Jia, Z., Yu, Y., Hou, S., and Wang, L. (2019). Biomimetic architected materials with improved dynamic performance. J. Mech. Phys. Solid. *125*, 178–197.
39. Bolmin, O., Socha, J.J., Alleyne, M., Dunn, A.C., Fezzaa, K., and Wissa, A.A. (2021). Nonlinear elasticity and damping govern ultrafast dynamics in click beetles. Proc. Natl. Acad. Sci. USA *118*. e2014569118.
40. Li, X.-W., Ji, H.-M., Yang, W., Zhang, G.-P., and Chen, D.-L. (2017). Mechanical properties of crossed-lamellar structures in biological shells: a review. J. Mech. Behav. Biomed. Mater. *74*, 54–71.
41. Speck, O., and Spatz, H.C. (2004). Damped oscillations of the giant reed Arundo donax (Poaceae). Am. J. Bot. *91*, 789–796.
42. Jiao, D., Liu, Z.Q., Zhu, Y.K., Weng, Z.Y., and Zhang, Z.F. (2016). Mechanical behavior of mother-of-pearl and pearl with flat and spherical laminations. Mater. Sci. Eng. C Mater. Biol. Appl. *68*, 9–17.
43. Liu, Z., Xu, X., and Tang, R. (2016). Improvement of biological organisms using functional material shells. Adv. Funct. Mater. *26*, 1862–1880.
44. Tang, C., Du, B., Jiang, S., Shao, Q., Dong, X., Liu, X.-J., and Zhao, H. (2022). A pipeline inspection robot for navigating tubular environments in the sub-centimeter scale. Sci. Robot. *7*, eabm8597.
45. Ze, Q., Wu, S., Nishikawa, J., Dai, J., Sun, Y., Leanza, S., Zemelka, C., Novelino, L.S., Paulino, G.H., and Zhao, R.R. (2022). Soft robotic origami crawler. Sci. Adv. *8*, eabm7834.